Hybrid Modelling, Control and Simulation of Knee Joint Actuated by Antagonistic Pneumatic Artificial Muscles

Jessica Magdy[1,2,*], Omar M. Shehata[1,2], Hamdy A. Kandil[1], and ElSayed I. Morgan[1,2]

[1] Mechatronics Engineering Department, Faculty of Engineering and Materials Science, German University in Cairo, Egypt
[2] Multi-Robot Systems (MRS) Research Group, Cairo, Egypt
Email: jessica.gergis@guc.edu.eg (J.M.); omar.mohamad@guc.edu.eg (O.M.S.); hamdy.kandil@guc.edu.eg (H.A.K.); elsayed.morgan@guc.edu.eg (E.I.M.)
*Corresponding author

***Abstract*—This article presents a hybrid model and control strategy for a knee joint actuated by antagonistic McKibben pneumatic artificial muscles. The approach integrates a static force model, which captures the relationship between muscle contraction ratio and internal pressure, and a dynamic model that accounts for friction effects. A compressible flow model describes how pressure is established within each muscle during inflation and released during deflation. By unifying these elements with a differential equation for the knee joint's motion, a comprehensive representation of the system is developed. The accuracy of the model was validated against published experimental data for two different McKibben muscles, achieving Normalized Root Mean Square Errors (NRMSE) between 3.39% and 6.46% under various validation scenarios. A Proportional–Integral–Derivative (PID) controller manages the discrepancy between the reference trajectory and the actual knee angle, adjusting the valve orifice area to regulate airflow accordingly. The system's closed-loop performance is evaluated using multiple trajectories—including square wave, triangular, sine wave, and a human gait cycle—quantified through root mean square of the tracking error, the highest absolute deviation recorded, and the normalized error expressed as a percentage of the total motion span. Findings indicate that this methodology provides a robust basis for future advancements in pneumatic actuation for robotics applications.**

***Keywords*—pneumatic artificial muscles, bipedal robot, knee joint, hybrid modelling, antagonistic actuation, dynamic system simulation, Proportional–Integral–Derivative (PID) controller, trajectory tracking**

I. Introduction

Traditional actuators, such as electric or hydraulic actuators, often face limitations in achieving lightweight structures and providing natural joint compliance. Pneumatic Artificial Muscles (PAMs) present a promising actuation approach, particularly due to their ability to deliver high power relative to their weight, their inherent compliance for absorbing physical impacts, and their functional resemblance to biological muscles. By exploiting the inflation and deflation of an internal bladder encased in a braided mesh, McKibben muscles can generate contractile forces that mimic the behavior of skeletal muscle tissue, making them particularly attractive for exoskeletons, prosthetic devices, and humanoid or bipedal robots [1–8].

One of the earliest works establishing the fundamental principles of McKibben muscles was conducted by Chou and Hannaford [9], who introduced a static modeling approach describing the force–length–pressure relationship. Later contributions expanded this to include frictional phenomena and non-ideal geometric effects, which are vital in capturing real-world performance [10, 11]. Tondu and Lopez emphasized that braided pneumatic muscles can exhibit complex behaviors under dynamic loading, necessitating refined models that incorporate friction effect [10]. The inclusion of fluid dynamics is also essential, as inflation and deflation processes under varying pressures significantly impact muscle contraction speed and model accuracy [12]. These considerations become even more critical in antagonistic setups, where two muscles acting as flexor and extensor must be carefully pressurized to achieve joint motion and stiffness control.

The notion of antagonistic actuation takes inspiration directly from biology, which muscles operate in opposing pairs to move skeletal joints. Antagonistic PAM systems have been explored for upper-limb rehabilitation devices, walking-assist exoskeleton, and even bipedal robots [13–15]. However, the dynamic nature of these systems introduces several modeling and control challenges. For example, friction from the braided structure can vary with contraction speed and the air compressibility must be captured accurately for realistic simulations These complexities demand an integrated

Manuscript received January 28, 2025; revised March 20, 2025; accepted April 30, 2025; published August 6, 2025.

modeling approach, merging static force relations, friction models, and compressible flow equations, thus enabling engineers to accurately estimate the behavior of robotic platform actuated by antagonistic pneumatic muscle.

From a control perspective, Proportional–Integral–Derivative (PID) algorithms have long been the mainstay in industrial and robotic applications [16]. PID control has been widely utilized in controlling pneumatic actuators and McKibben muscles across various applications [17–20]. In addition to PID, other control strategies have also been actively explored in recent research. Sliding-mode control techniques have been proposed for their robustness and precise tracking capabilities in PAM-actuated manipulators, as demonstrated in the development of optimal and super-twisting sliding mode controllers [21–23]. Optimization techniques have also attracted interest in recent studies, particularly for tuning controller parameters to enhance performance and robustness in systems [24–26]. Intelligent control approaches like adaptive and fuzzy logic controllers continue to be explored for handling the nonlinear and dynamic nature of soft actuators [27–29]. Nevertheless, PID remains an attractive solution due to its simplicity, ease of implementation, and straightforward tuning process.

This paper aims to present an integrated modeling and control framework for a knee joint actuated by antagonistic McKibben muscles. It begins in second section by reviewing the static model of Mckibben muscle. Building on this, a dynamic model, followed by a fluid dynamic model and then the antagonistic knee-joint equation then combines these elements into a comprehensive representation Section III provides model validation, while Section IV introduces the PID controller used for trajectory tracking. In Section V, simulation results are presented and evaluated under different reference trajectories. Finally, the paper ends with a conclusion section.

II. Modeling of Knee Joint

A. Static Modelling of Mckibben Artificial Muscle

McKibben muscle typically consists of an inflatable inner bladder—commonly manufactured from an elastic material such as rubber—enclosed by a braided mesh, often composed of high-strength fibers like nylon. When compressed air is supplied to the inner bladder, it expands radially while contracting axially, resulting in a force that pulls axially in a manner analogous to that of biological muscles. This contraction force can be modulated through varying the internal air pressure, offering a smooth and compliant actuation.

There are several models to model the relation between the contraction force, internal pressure inside the muscle and muscle length some of the analytically and others experimentally. One of the most widely referenced models in the literature describes the force generated by the muscle in terms of its contraction ratio and internal pressure. This model is derived using the virtual work principle, under the assumption that the muscle maintains a cylindrical geometry during inflation and deflation, and that no energy is lost in the process [3]. Therefore, the work done by the internal air pressure over volume expansion is equal to the work done by the axial force over muscle length reduction as in Eq. (1).

$$P\delta V = -F\delta L \tag{1}$$

where P is air pressure, δV is muscle's volume variation, F is the axial force, and δL is muscle's length variation.

The derivation proceeds by splitting the pressure forces into axial and lateral components and incorporating equations that link the muscle's length and radius to their initial values, yielding the final expression shown in Eq. (2).

$$f(P,\epsilon) = \pi r_o^2 P[a(1-k\epsilon)^2 - b] \tag{2}$$

where $\epsilon = \frac{l_o - l}{l_0}$, $a = \frac{3}{tan^2\alpha_o}$, and $b = \frac{1}{sin^2\alpha_o}$.
where ϵ is the contraction ratio, l_o is intial muscle length, r_o is intial muscle radius, α_o is initial braid angle, and k is the correction factor.

The original model does not introduce the correction factor k. This factor was later incorporated to improve the accuracy of the force estimation by addressing the geometric simplification in the original model, which assumes a perfectly cylindrical shape, whereas in practice the muscle adopts a conical profile at both ends during inflation [10].

B. Dynamic Modelling of Mckibben Artificial Muscle

The dynamic force exerted by the muscle is a relation between force, contraction ratio, rate of contraction ratio and the pressure inside the muscle. The PAM's dynamic component of force is mostly caused by hydrodynamic friction between nylon threads and thread-on-tube friction. Researchers commonly express this using both viscous and Coulomb friction in the model [30]. The complete dynamic model is combination between static force model and friction model as in Eq. (3).

$$F(P,\epsilon,\dot{\epsilon}) = f(P,\epsilon) - C_v\dot{\epsilon} - C_c sgn(\epsilon) \tag{3}$$

where C_v viscous friction coefficient, and C_c coulomb friction coefficient.

The inputs of that model are the contraction ratio, its rate of change, and the internal pressure, which is computed using the flow model.

C. Fluid Dynamic Modeling

The objective of the flow model is to describe how the pressure builds inside the muscle during inflation and how it reduces during deflation. That can be archived by modelling the compressible flow through a valve orifice. Eqs. (4) and (5) described the mass flow rate through the orifice during subsonic and choked flow regions [31].

$$\dot{m} = A \cdot C \cdot \Psi \cdot P_1 \sqrt{\frac{2}{R \cdot T_1}} \tag{4}$$

$$\psi = \begin{cases} \sqrt{\frac{\gamma}{\gamma-1}\left[\left(\frac{P_2}{P_1}\right)^{\frac{2}{\gamma}} - \left(\frac{P_2}{P_1}\right)^{\frac{\gamma+1}{\gamma}}\right]} & \text{for } \frac{P_2}{P_1} > p_r \text{(subsonic flow)} \\ \left(\frac{2}{\gamma+1}\right)^{\frac{1}{\gamma-1}}\sqrt{\frac{\gamma}{\gamma+1}} & \text{for } \frac{P_2}{P_1} \le p_r \text{ (choked flow)} \end{cases} \quad (5)$$

where $\dot{m}$ mass flow rate, A is effective orifice area, C is discharge coefficient, R is gas constant, T_1 is upstream temperature, P_1 is absolute upstream pressure, P_2 is absolute downstream pressure, ψ is flow function, γ is specific heat ratio, and p_r is critical pressure ratio.

The critical pressure ration equals 0.528. The upstream pressure in case inflation is equal to the setting of pressure regulator of the compressor assuming no losses in hoses while the downstream pressure is muscle pressure. In contrast during deflation upstream pressure is muscle pressure and downstream pressure is atmospheric pressure.

Assuming that air behaves as a perfect gas, a common assumption in numerous pneumatic system models [12, 30, 32, 33], the ideal gas law can be appropriately applied. By taking the time derivative of the ideal gas law and considering isothermal conditions for the inflation and deflation processes, the following expression is derived.

$$\dot{P} = \frac{RT\dot{m} - \dot{V}P}{V} \quad (6)$$

where $\dot{p}$ is rate of change of muscle pressure, T is muscle's temperature, and V muscle's volume.

D. Dynamics of Antagonistic Actuation for Knee Joint

Antagonistic pneumatic artificial muscles offer a promising actuation method for knee joint movement. By configuring two pneumatic muscles in opposition as illustrated in Fig. 1—one acting as the flexor and the other as the extensor—the system can achieve joint motion and stiffness modulation in a more biomimetic manner than traditional rigid actuators. The key to this mechanism is balancing pressure between the two muscles: as one muscle inflates and pulls the joint in one direction, the other muscle is partially depressurized but still maintains some tension. These two forces generate the required torque for the knee joint which can be represented by the following equation of motion.

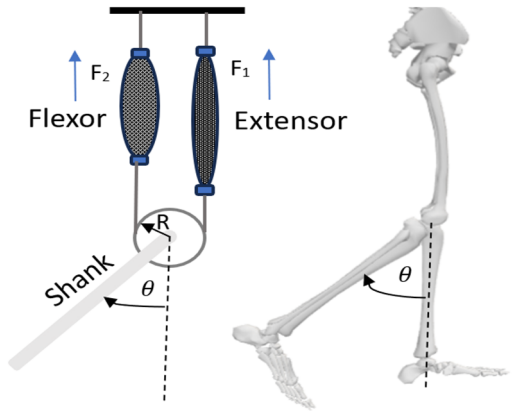

Fig. 1. Knee joint powered by antagonistic pneumatic artificial muscle.

$$I\ddot{\theta} = (F_1 - F_2)R - \frac{1}{2}mgl\sin\theta \quad (7)$$

where I is the system's rotational inertia, θ is rotational displacement of the joint, F_1 and F_2 are dynamic force of each muscle according to Eq. (3), R is pully radius, m is shank mass, and l is shank length.

Dynamic force generated by each muscle depends on its internal pressure. During calculation the pressure variance using Eq. (6) commonly the rate of change of volume is neglected and the volume considered as constant number [30, 32], But in that model the change of muscle volume is taken into consideration. The volume of the 2 muscles is driven as a function of angular displacement as in
Eqs. (8)–(13).

$$V_1 = \left(\frac{\pi r_o^2}{sin^2(\alpha_o)}\right) \cdot (A\theta^3 + B\theta^2 + C\theta + D) \quad (8)$$

$$V_2 = \left(\frac{\pi r_o^2}{sin^2(\alpha_o)}\right) \cdot (-A\theta^3 + B\theta^2 - C\theta + D) \quad (9)$$

where V_1 and V_2 are volume of first and second muscles respectively. The terms A through D represent coefficients and can be expressed as follows.

$$A = \frac{1}{l_o^2} \cdot (R^3 cos^2(\alpha_o)) \quad (10)$$

$$B = \frac{1}{l_o} \cdot (2\epsilon_o R^2 cos^2(\alpha_o) - 3R^2 cos^2(\alpha_o)) \quad (11)$$

$$C = R \cdot (3cos^2(\alpha_o) - 6\epsilon_o cos^2(\alpha_o) + 3\epsilon_o^2 cos^2(\alpha_o) - 1) \quad (12)$$

$$D = l_o \cdot (1 - cos^2(\alpha_o) + 3\epsilon_o cos^2(\alpha_o) - 3\epsilon_o^2 cos^2(\alpha_o) - \epsilon_o + \epsilon_o^3 cos^2(\alpha_o)) \quad (13)$$

where ϵ_O is the initial contraction ratio of each muscle. Those equations are valid by assuming that both muscles are identical.

III. Model Validation

To ensure that the presented model accurately represents the physical behavior of pneumatic artificial muscles, the dynamic and fluid dynamic models were validated against experimentally published data [10, 32]. Two different McKibben muscles, subjected to distinct loading conditions and varying input pressures, were used for validation to assess the model's accuracy.

The first muscle examined had an initial length of 30 cm and a radius of 7 mm. Two separate tests were conducted: in the first scenario, the muscle carried a load of 30 kg and received an input supply pressure of 4 bar, while in the

second scenario, the load was 20 kg and the input supply pressure was 3 bar. The experimental data consist of the position of the load as it was lifted by the muscle over time. As illustrated in Fig. 2(a), the model-generated data closely match the experimentally measured muscle behavior under the 30 kg load at 4 bar input pressure. Similarly, Fig. 2(b) shows the model and the experimental data for the second loading scenario (20 kg load, 3 bar pressure). The solid red line represents the measured experimental data, while the dashed blue line shows the simulation results of the pneumatic muscle model under the same conditions as the experiment. The Normalized Root Mean Square Errors (NRMSE) in these cases were computed as 5.2% for the first scenario and 5.3% for the second loading conditions, demonstrating a high level of accuracy and validating the model's reliability under varying operational conditions.

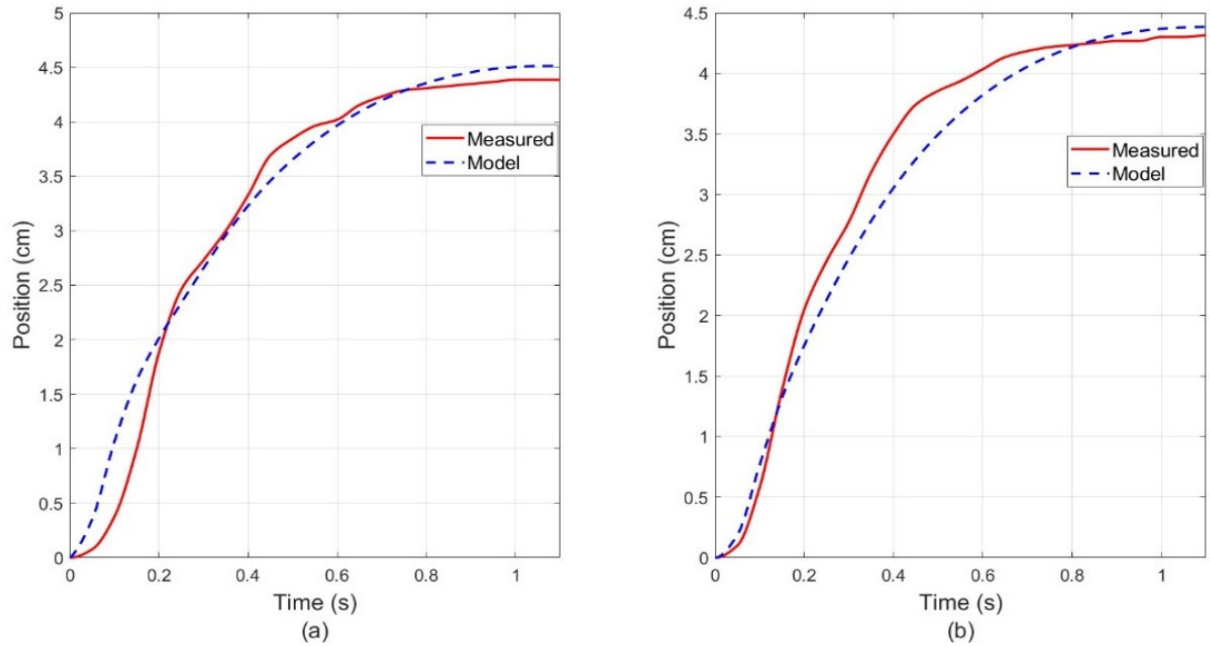

Fig. 2. Comparison of model results with experimental measurements for the first McKibben muscle under two different loading scenarios: (a) Muscle behavior with a 30 kg load and 4 bar input pressure; (b) Muscle behavior with a 20 kg load and 3 bar input pressure.

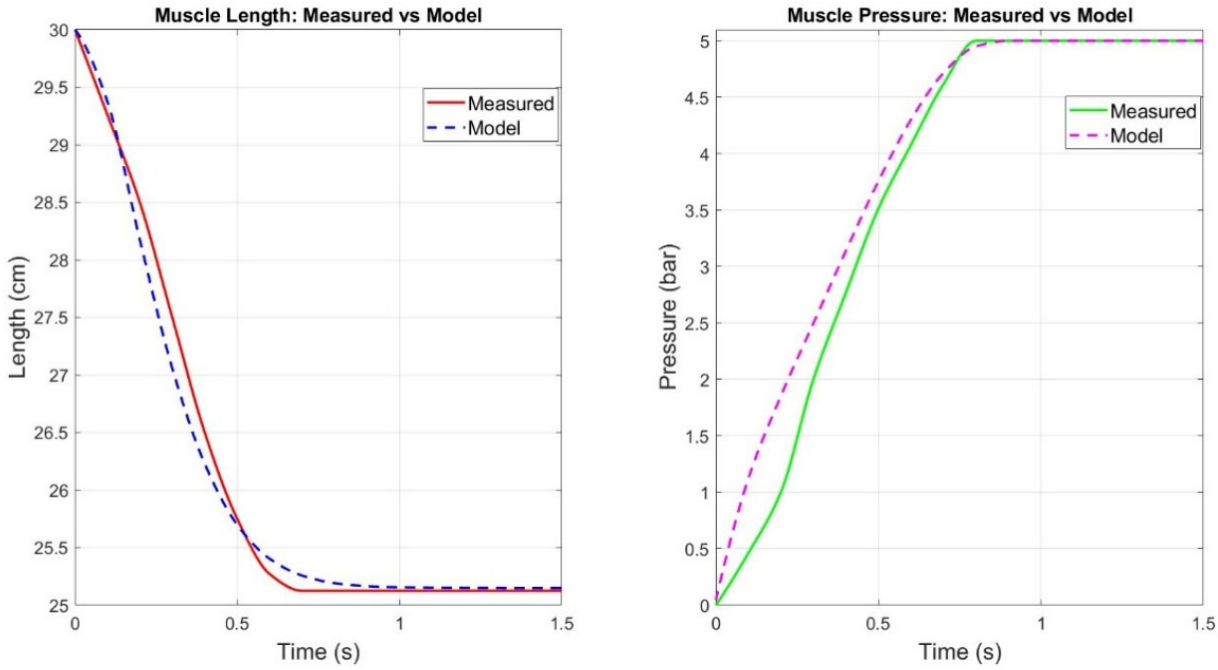

Fig. 3. Validation of the model against experimental data for the second McKibben muscle under a load of 1.5 kg and an input supply pressure of 5 bar.

Further validation was performed using a second McKibben muscle, with an initial length of 30 cm, loaded with 1.5 kg and subjected to an input supply pressure of 5 bar. As shown in Fig. 3, comparisons of the measured muscle length and internal pressure against the model data again confirm the accuracy of the presented model. The NRMSE values calculated for the muscle length and internal pressure were found to be 3.39% and 6.46%, respectively. These validation results confirm the model's capability to accurately represent real-world pneumatic muscle behavior.

IV. Control of Knee Joint

Proportional–Integral–Derivative (PID) controllers have long been recognized as a fundamental control strategy across numerous engineering applications, owing to their relatively straightforward implementation and broad applicability [16, 34]. The control action is derived from three distinct elements: the proportional term addresses the instantaneous error, the integral term accounts for the accumulated error, and the derivative term considers the error's rate of change. Multiple studies in the literature have demonstrated the effective performance of PID controllers when applied to pneumatic actuators and McKibben muscles, showing reliable and accurate trajectory tracking [17–20]. In this knee-joint actuation system, the PID controller processes the difference between the reference angle (the desired knee position) and the joint angle, generating an output command that adjusts the proportional valve to regulate airflow into the antagonistic pneumatic artificial muscles. This setup enables each muscle to respond according to the control requirements and ensures that the joint angle tracks the specified reference. Fig. 4 shows the block diagram representing the hybrid model and control of the knee joint.

V. Simulation Results

In this section, the McKibben pneumatic muscle's static model and the hybrid knee-joint model are simulated using Simulink. This step is aimed at evaluating the derived equations under various operating conditions and validating both the mechanical and control aspects of the system in a software environment. The static model of a muscle is validated against article [10] in references section.

A. Simulation of Static Modelling of Mckibben Artificial Muscle

Fig. 5 illustrates static force behavior of the McKibben muscle as a function of contraction ratio under five isobaric scenarios. The muscle's parameters are set to 30 cm in length, 7 mm in radius, an initial braid angle of 20° and 1.3 correction factor. Each curve in the figure demonstrates how varying the internal pressure alters the muscle's capacity to produce force at different levels of contraction.

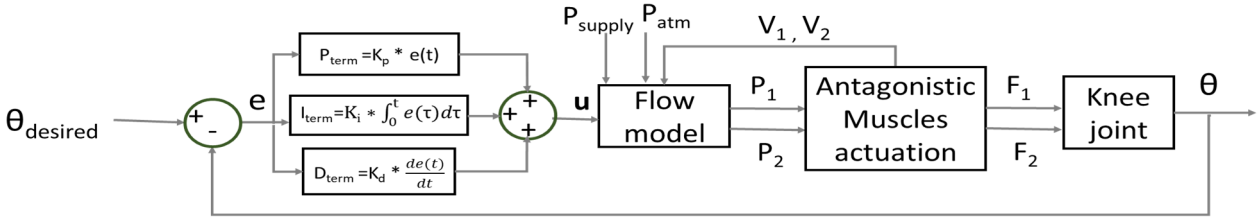

Fig. 4. Block diagram of integrated model and control of Knee joint.

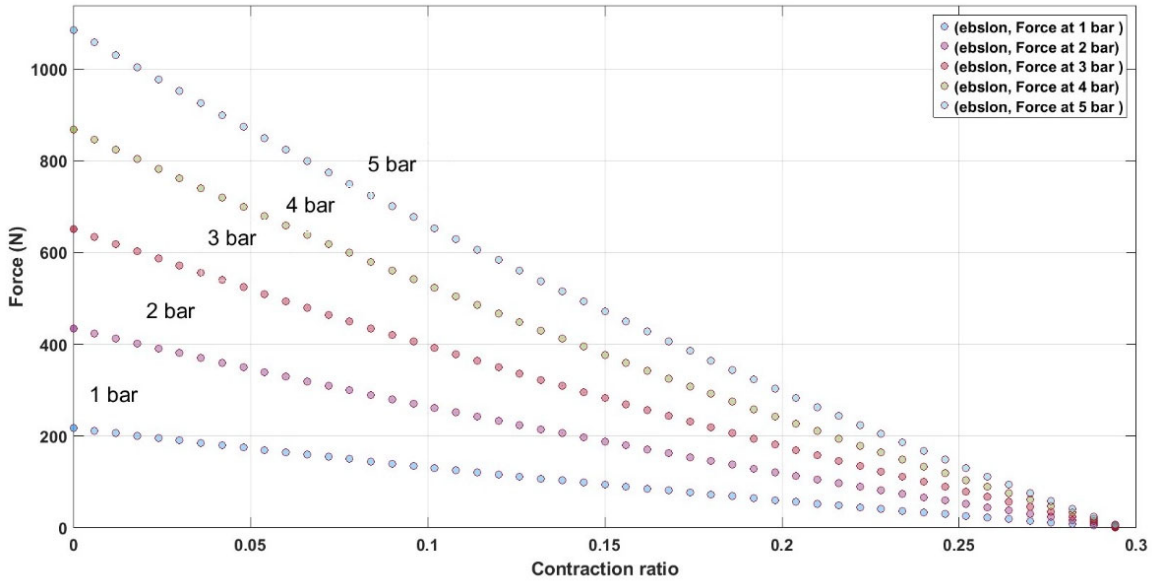

Fig. 5. Simulation result of static force model of Mckibben muscle at five isobaric conditions.

B. Simulation of Dynamics of Knee Joint

The hybrid model, which integrates knee joint dynamics with the actuator dynamics including the flow model was simulated, and the corresponding closed-loop responses under various trajectory inputs are presented in Fig. 6. Specifically, the system's performance is illustrated for different trajectories: square wave, triangular, and sine wave trajectory. The solid yellow curves are the reference trajectories while the bule dashed curves are the system responses. Table I provides the values of the model parameters used in these simulations. All simulation parameters were carefully selected to reflect realistic humanoid robot dimensions, such as appropriate shank length. Specifically, the pneumatic muscle length was determined to ensure the desired knee-joint angles could be achieved without exceeding the muscle's maximum contraction ratio. Furthermore, the input supply pressure was chosen to operate within safe and practical limits, thereby ensuring reliable and stable system behavior.

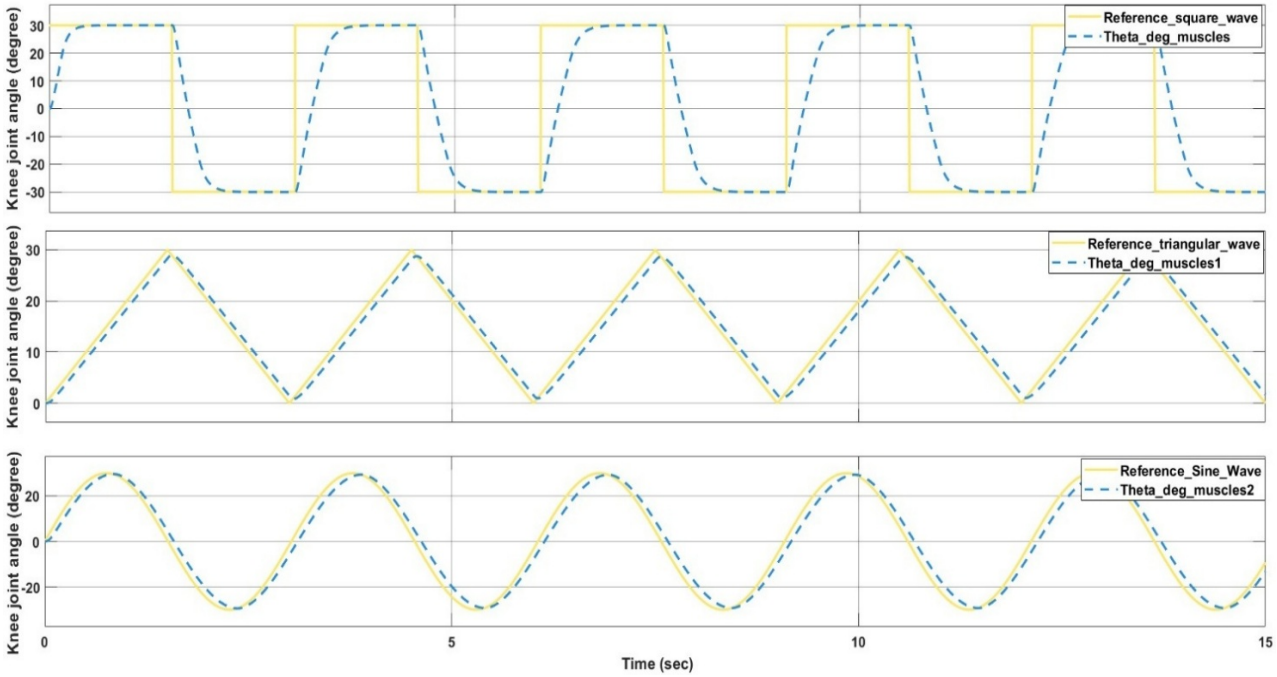

Fig. 6. Simulated closed-loop performance of the knee joint for various input trajectories.

TABLE I. VALUES OF MODEL PARAMETERS USED IN THE SIMULATION

Parameter	Value
Muscle's length	30 cm
Muscle's initial radius	1 cm
Initial braid angle	20º
Pully's radius	4 cm
Shank mass	1 kg
Shank length	40 cm
Temperature	300 k
Gas constant	287 J/kg·K
Air supply pressure	6 bar
Atmospheric pressure	1 bar

Fig. 7 illustrates the system's response when tracking a knee trajectory derived from a normal human gait cycle. The graph includes both the desired and actual joint angles, as well as the resulting error between them, providing a visual representation of how effectively the model follows typical gait motion under closed-loop control. The reference knee trajectory is represented as discrete values, with the trajectory planner transmitting the desired angle at specific time intervals.

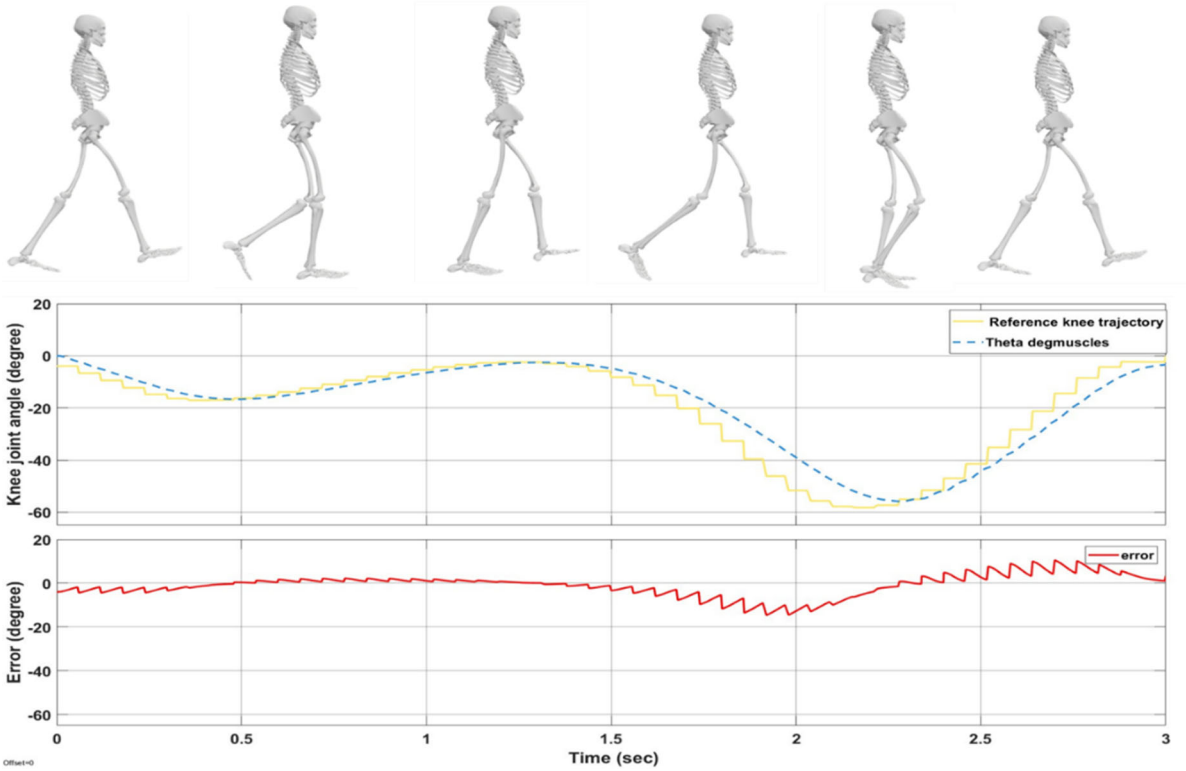

Fig. 7. System response of the knee joint while following a human walking pattern.

C. Performance Evaluation

The performance of the knee joint's closed-loop response is assessed by computing quantitative error metrics for each of the four discussed trajectories. These metrics include the Root Mean Square Error (RMSE), Maximum Absolute Error (MAE), and a percentage-based normalized RMSE (NRMSE). The RMSE provides an overall measure of the average deviation between the desired and actual joint angles, while the MAE highlights the largest deviation encountered during the trajectory tracking. The NRMSE, expressed as a percentage of the range of motion, offers a normalized evaluation of the system performance, making it suitable for comparing different trajectories. Table II presents the calculated values of RMSE, MAE, and NRMSE, illustrating the system performance for the square wave, triangular, sine wave, and human gait trajectory.

TABLE II. ERROR METRICS (RMSE, MAE, NRMSE) FOR DIFFERENT TRAJECTORIES

Trajectory	RMSE	MAE	NRMSE %
Square wave	19.21	60.04	32.017
Triangular	1.54	2.2	5.133
Sine wave	3.593	5.305	5.988
Human gait	5.146	14.66	9.193

The controlled knee joint response demonstrates the ability to track all the discussed trajectories with NRMSE less than 10%, except for the square wave trajectory. The triangular trajectory exhibited the lowest NRMSE (5.133%) and maximum absolute error (MAE = 2.2°), indicating highly accurate tracking performance. It has gradual and continuous changes in the reference angle. Similarly, the sine wave trajectory, characterized by smooth and periodic angle variations, showed satisfactory tracking accuracy with an NRMSE of 5.988% and a maximum absolute error of 5.305°. The human gait trajectory, which represents realistic joint movements was tracked effectively by the system with an NRMSE of 9.193% and a maximum absolute error of approximately 14.66°. In contrast, the square wave trajectory presented a notably higher NRMSE (32.017%) and maximum absolute error (60.04°). This outcome was expected due to the sudden discontinuities in the reference trajectory, where the reference abruptly switches from +30° to −30°. Such discontinuities inherently induce large transient errors, which contribute to the maximum absolute error reaching 60.04° and significantly increase the overall root mean square error. Despite these instantaneous errors, the system consistently reached the target angles after short transient periods. This analysis highlights that the PID control provides a suitable balance between simplicity, computational efficiency, and tracking performance for knee joint actuated by pneumatic muscles.

VI. CONCLUSION AND FUTURE WORK

This study presented a comprehensive approach to modeling and controlling a knee joint actuated by antagonistic McKibben artificial muscles. The modeling component integrated the static force characteristics, dynamic friction behavior, and compressible fluid dynamics associated with the muscles, while the knee joint's motion was captured through a differential equation that accounts for torque and load effects. The validity of the presented model was confirmed by comparison with published experimental data of pneumatic muscle behavior,

yielding low normalized root mean square errors (3.39%–6.46%) across multiple testing scenarios. A PID controller was employed to track various reference trajectories by regulating the proportional valve connected to the muscles. Simulation results demonstrated that the system could effectively follow most trajectories including square wave, triangular, sine wave, and human gait patterns. Overall, the results confirm that PID control provides an effective balance of simplicity and performance for PAM-actuated joints.

As a direction for future work, the system could be expanded to handle real-time environmental disturbances, thereby enhancing its applicability in scenarios requiring adaptive gait control. This can be achieved by implementing adaptive and robust control algorithms capable of adjusting controller parameters dynamically in response to changes in system behavior. Such an approach would significantly enhance the system's robustness under varying environmental uncertainties.

Conflict of Interest

The authors declare no conflict of interest.

Author Contributions

Jessica Magdy suggested the idea of the research, established mathematical modeling, performed simulations, validated the results, and prepared the initial manuscript draft. Omar M. Shehata contributed to control system design, oversaw the validation process, and contributed to manuscript editing and refinement. Hamdy A. Kandil provided expertise on pneumatic systems and contributed to manuscript refinement. ElSayed I. Morgan supervised the research methodology, provided technical guidance, and contributed to manuscript revision. All authors reviewed and approved the final manuscript for publication.

References

[1] B. Jamil, N. Oh, J. G. Lee, H. Lee, and H. Rodrigue, "A review and comparison of linear pneumatic artificial muscles," *Int. J. Precis. Eng. Manuf.-Green Technol.*, vol. 11, no. 1, pp. 277–289, 2024.

[2] B. Kalita, A. Leonessa, and S. K. Dwivedy, "A review on the development of pneumatic artificial muscle actuators: Force model and application," *Actuators*, vol. 11, no. 10, 288, 2022.

[3] C. P. Chou and B. Hannaford, "Measurement and modeling of McKibben pneumatic artificial muscles," *IEEE Trans. Robot. Autom.*, vol. 12, no. 1, pp. 90–102, 1996.

[4] M. A. Sarhan, S. Shihab, B. E. Kashem, and M. Rasheed, "New exact operational shifted Pell matrices and their application in astrophysics," in *Proc. J. Phys.: Conf. Ser.*, 2021, vol. 1879, no. 2, 022122.

[5] D. Bouras, M. Rasheed, R. Barille, and M. N. Aldaraji, "Efficiency of adding DD3+ (Li/Mg) composite to plants and their fibers during the process of filtering solutions of toxic organic dyes," *Opt. Mater.*, vol. 131, 112725, 2022.

[6] A. D. D. R. Carvalho, N. Karanth, and V. Desai, "Characterization of pneumatic muscle actuators and their implementation on an elbow exoskeleton with a novel hinge design," *Sens. Actuators Rep.*, vol. 4, 100109, 2022.

[7] M. Rasheed, M. N. Al-Darraji, S. Shihab, A. Rashid, and T. Rashid, "Solar PV modelling and parameter extraction using iterative algorithms," in *Proc. J. Phys.: Conf. Ser.*, 2021, vol. 1963, no. 1, 012059.

[8] B. Tondu and P. Lopez, "The McKibben muscle and its use in actuating robot arms showing similarities with human arm behavior," *Ind. Robot: Int. J.*, vol. 24, no. 6, pp. 432–439, 1997.

[9] C. P. Chou and B. Hannaford, "Static and dynamic characteristics of McKibben pneumatic artificial muscles," in *Proc. 1994 IEEE Int. Conf. Robot. Autom.*, 1994, pp. 281–286.

[10] B. Tondu and P. Lopez, "Modeling and control of McKibben artificial muscle robot actuators," *IEEE Control Syst. Mag.*, vol. 20, no. 2, pp. 15–38, 2000.

[11] M. Doumit, A. Fahim, and M. Munro, "Analytical modeling and experimental validation of the braided pneumatic muscle," *IEEE Trans. Robot.*, vol. 25, no. 6, pp. 1282–1291, 2009.

[12] B. S. Kang, C. S. Kothera, B. K. Woods, and N. M. Wereley, "Dynamic modeling of McKibben pneumatic artificial muscles for antagonistic actuation," in *Proc. 2009 IEEE Int. Conf. Robot. Autom.*, Japan, 2009, pp. 182–187.

[13] H. Chi, H. Su, W. Liang, and Q. Ren, "Control of a rehabilitation robotic device driven by antagonistic soft actuators," *Actuators*, vol. 10, no. 6, 123, 2021.

[14] D. P. Ferris, J. M. Czerniecki, and B. Hannaford, "An ankle-foot orthosis powered by artificial pneumatic muscles," *J. Appl. Biomech.*, vol. 21, no. 2, pp. 189–197, 2005.

[15] B. Verrelst, R. Van Ham, B. Vanderborght, F. Daerden, D. Lefeber, and J. Vermeulen, "Lucy, a bipedal walking robot with pneumatic artificial muscles," *Auton. Robots*, vol. 18, no. 2, pp. 201–213, 2004.

[16] R. P. Borase, D. K. Maghade, S. Y. Sondkar, and S. N. Pawar, "A review of PID control, tuning methods, and applications," *Int. J. Dyn. Control*, vol. 9, pp. 818–827, 2021.

[17] G. A. Muzy and A. S. Caporali, "Positioning system of a pneumatic actuator driven by proportional pressure regulator valves," in *Proc. 4th Workshop on Innovative Engineering for Fluid Power (WIEFP)*, 2018, pp. 28–30.

[18] N. H. Sunar, M. F. Rahmat, Z. H. Ismail, A. M. Faudzi, S. N. S. Salim, and S. I. Samsudin, "Application of optimization technique for PID controller tuning in position tracking of pneumatic actuator system," in *Proc. 2013 IEEE 9th Int. Colloq. Signal Process. Appl.*, 2013, pp. 33–38.

[19] K. Yokoyama and K. Kogiso, "PID position control of McKibben pneumatic artificial muscle using only pressure feedback," in *Proc. 2018 Annu. Am. Control Conf. (ACC)*, 2018, pp. 3362–3367.

[20] X. Zang, Y. Liu, S. Heng, Z. Lin, and J. Zhao, "Position control of a single pneumatic artificial muscle with hysteresis compensation based on modified Prandtl–Ishlinskii model," *Biomed. Mater. Eng.*, vol. 28, no. 2, pp. 131–140, 2017.

[21] M. E. Sadiq, A. J. Humaidi, S. K. Kadhim, A. Al Mhdawi, A. Alkhayyat, and I. K. Ibraheem, "Optimal sliding mode control of single arm PAM-actuated manipulator," in *Proc. 2021 IEEE 11th Int. Conf. Syst. Eng. Technol. (ICSET)*, 2021, pp. 84–89.

[22] A. Falah, A. J. Humaidi, A. Al-Dujaili, and I. K. Ibraheem, "Robust super-twisting sliding control of PAM-actuated manipulator based on perturbation observer," *Cogent Eng.*, vol. 7, no. 1, 1858393, 2020.

[23] A. J. Humaidi, S. K. Kadhim, M. E. Sadiq, S. J. Abbas, A. Q. Al-Dujaili, and A. R. Ajel, "Design of optimal sliding mode control of PAM-actuated hanging mass," *ICIC Express Lett.*, vol. 16, no. 11, pp. 1193–1204, 2022.

[24] A. J. Humaidi, A. A. Oglah, S. J. Abbas, and I. K. Ibraheem, "Optimal augmented linear and nonlinear PD control design for parallel robot based on PSO tuner," *Int. Rev. Model. Simul.*, vol. 12, no. 5, pp. 281–291, 2019.

[25] A. J. Humaidi and A. I. Abdulkareem, "Design of augmented nonlinear PD controller of Delta/Par4-like robot," *J. Control Sci. Eng.*, vol. 2019, no. 1, 7689673, 2019.

[26] A. F. Hasan, N. Al-Shamaa, S. S. Husain, A. J. Humaidi, and A. Al-Dujaili, "Spotted hyena optimizer enhances the performance of fractional-order PD controller for tricopter drone," *Int. Rev. Appl. Sci. Eng.*, vol. 15, no. 1, pp. 82–94, 2024.

[27] Q. T. Dao, M. L. Nguyen, and S. I. Yamamoto, "Discrete-time fractional order integral sliding mode control of an antagonistic actuator driven by pneumatic artificial muscles," *Appl. Sci.*, vol. 9, no. 12, 2503, 2019.

[28] N. Sun, D. Liang, Y. Wu, Y. Chen, Y. Qin, and Y. Fang, "Adaptive control for pneumatic artificial muscle systems with parametric uncertainties and unidirectional input constraints," *IEEE Trans. Ind. Informat.*, vol. 16, no. 2, pp. 969–979, 2019.

[29] H. Jahanabadi, M. Mailah, M. Z. Md Zain, and H. M. Hooi, "Active force with fuzzy logic control of a two-link arm driven by pneumatic artificial muscles," *J. Bionic Eng.*, vol. 8, no. 4, pp. 474–484, 2011.
[30] S. Ganguly, A. Garg, A. Pasricha, and S. Dwivedy, "Control of pneumatic artificial muscle system through experimental modeling," *Mechatronics*, vol. 22, no. 8, pp. 1135–1147, 2012.
[31] P. Beater, *Pneumatic Drives: System Design, Modelling and Control*, Berlin: Springer, 2007.
[32] J. Mi, G. Huang, and J. Yu, "Characterization and joint control study of pneumatic artificial muscles," *Appl. Sci.*, vol. 13, no. 2, 1075, 2023.
[33] M. D. Doumit and S. Pardoel, "Dynamic contraction behavior of pneumatic artificial muscle," *Mech. Syst. Signal Process.*, vol. 91, pp. 93–110, 2017.
[34] R. Chen, "A comprehensive analysis of PID control applications in automation systems: Current trends and future directions," *Highl. Sci. Eng. Technol.*, vol. 97, 2024.